Solar Energy Materials & Solar Cells 289 (2025) 113655

Contents lists available at ScienceDirect

Solar Energy Materials and Solar Cells

journal homepage: www.elsevier.com/locate/solmat

Design and characterization of a SiO_2-TiO_2 coating containing organic and inorganic thermochromic pigments and optimized with TiO_2-P25 for improved long-term performance in energy-efficient roofing

Ana Carolina Hidalgo-Araujo [a,c], Rafael Salomão [b], Umberto Berardi [c,d,*], Kelen Almeida Dornelles [a]

[a] Institute of Architecture and Urbanism, University of São Paulo (USP), Brazil
[b] São Carlos School of Engineering, Materials Engineering Department, USP, Brazil
[c] Architectural Science, Toronto Metropolitan University, TMU, Toronto, Canada
[d] Department of Civil Engineering and Architectural Sciences, Politecnico di Bari, Italy

ARTICLE INFO

Keywords:
Adaptive materials
Laboratory testing
Building envelope
Building material

ABSTRACT

This experimental study focuses on developing and characterizing thermochromic roof coatings contributing to energy-efficient building solutions. It addresses two key challenges: the limited durability of organic thermochromic pigments and the lack of research on applying thermochromic materials to opaque surfaces, especially inorganic pigments. Two coatings were developed: whereas the first contained a microencapsulated organic pigment (TC), the second used inorganic vanadium dioxide-based particles (VO_2-W). Both were applied to ceramic and fiber cement tiles with a formulation that combined a binder (colloidal silica, SiO_2) and titanium dioxide (TiO_2) to improve durability. The novelty of the paper was the addition of a TiO_2-P25 protective layer that retarded photodegradation and improved the long-term stability of the TC pigment. Coating components were evaluated using differential scanning calorimetry, solar reflectance, scanning electron microscopy, infrared spectroscopy, and X-ray diffraction. Coating performance was assessed regarding solar reflectance, thermal emissivity, and hydrophobicity. The results showed that the TC coating responded dynamically to temperature changes, indicating potential for improving buildings' thermal comfort and energy efficiency. On the other hand, the VO_2-W coating showed limited performance in the infrared. In particular, TC coatings with TiO_2-P25 exhibited 57 % less degradation below the transition temperature and 37 % less when heated. The main finding of this study demonstrated that TiO_2-P25 significantly improved the durability of organic thermochromic coatings, offering a promising strategy to reduce the need for artificial cooling, reduce CO_2 emissions, and mitigate the urban heat-island effect. The results also addressed critical gaps in the durability of organic thermochromic pigments and the application of inorganic pigments to opaque surfaces.

1. Introduction

The growing impact of climate change is leading to greater energy consumption in buildings, mainly due to a higher reliance and dependence on artificial climate control for thermal comfort. This effect increases greenhouse gas emissions and global warming in a vicious cycle [1]. To address this challenge, thermochromic materials have gained attention for their ability to dynamically regulate solar reflectance based on surface temperature and enhance energy performance in buildings. These materials became more reflective at higher temperatures, reducing heat absorption and reverting to lower solar reflectance in cooler conditions [2]. Unlike conventional white paints, also known as cool materials, which maintain a static thermal performance, thermochromic coatings can improve energy efficiency by reducing cooling during hot periods and minimizing heat loss during colder ones [3].

These dynamic materials can be divided into two types. The first dye-based pigments consist of organic dyes embedded in a polymer matrix that change color in response to temperature variation due to shifts in their molecular structure [4]. These pigments change from colored to transparent within a temperature range of typically 25–35 °C [5]. Such

* Corresponding author. Architectural Science, Toronto Metropolitan University, TMU, Toronto, Canada.
E-mail address: umberto.berardi@poliba.it (U. Berardi).

https://doi.org/10.1016/j.solmat.2025.113655
Received 13 March 2025; Received in revised form 17 April 2025; Accepted 18 April 2025
Available online 21 April 2025

dynamic behavior helps to mitigate the winter penalty often associated with conventional white materials, improving thermal performance, particularly in climates with significant seasonal temperature variations [6,7].

Several studies have highlighted the effectiveness of dye-based organic thermochromic pigments in reducing energy consumption in buildings. For example, Berardi et al. [8] reported an 8.9 % reduction in cooling demand and a 1.7 % reduction in winter heating demand in Toronto, Canada. Yuxuan et al. [9] estimated energy savings between 4.28 and 5.02 kWh/m^2, whereas Sánchez et al. [10] observed a 1–12 % reduction in annual energy consumption. Recent studies, such as Song et al. [11], documented energy savings of 17.8–43.0 MJ/m^2 and a 9.4–38.0 kg CO_2/m^2 reduction compared to asphalt roofs. Guo et al. [12] demonstrated a 20.3 % reduction in energy consumption using thermochromic hydrogels that maintained surface temperatures 7–10 °C lower than conventional coatings. In addition, de Azevedo et al. [13] recommended using thermochromic coatings in Brazilian schools to improve thermal comfort in different climates. In contrast, Kitsopoulou et al. [14] found energy savings ranging from 2.19 % to 17.13 % in Athens, with the highest reductions occurring during the cooling season.

However, dye-based thermochromic materials face a major limitation: their sensitivity to photodegradation, which raises concerns about long-term stability and durability. Hakami et al. [6] highlighted this issue, noting that organic thermochromic materials are susceptible to sunlight-induced degradation despite their promising potential. Similarly, Badino et al. [15] found that thermochromic coatings can reduce surface temperatures by up to 35 °C but may lose solar reflectance after just three days of natural exposure.

To enhance the durability of organic thermochromic pigments, researchers have explored the incorporation of silicon dioxide or silica (SiO_2) and titanium dioxide or titania (TiO_2) particles. For example, Hu and Yu [16] showed that adding TiO_2 nanoparticles in thermochromic coatings improved performance, achieving 7.7 % energy savings, 3.6 % cost reduction, and 28.5 % reduction in CO_2 emissions compared to conventional cool roofs. In another study, the same authors developed a poly(vinyl chloride)-based film with thermochromic dyes and TiO_2 nanoparticles that reduced internal surface temperatures by 3.5 °C for concrete roofs and 9–10 °C for plastic roofs [17]. Liu et al. [5] developed superhydrophobic thermochromic coatings using nano-SiO_2 that achieved energy savings of up to 6.76 % in extreme climates. Zhang et al. [18] developed thermochromic phase-change microcapsules with a sandwich shell, where a silica base and polymeric outer layer protected the thermochromic layer, ensuring durability and stability. Hussain et al. [19] improved hydration, compressive strength, and color stability using silica-coated *leuco* dye-based thermochromic pigments in Portland cement pastes. Cheng et al. [20] created self-cleaning superhydrophobic coatings that achieved 13.74 % energy savings in northern China, while maintaining functionality after mechanical, chemical, and UV exposure. Li et al. [21] synthesized thermochromic phase-change microcapsules with SiO_2 shells, increasing thermal conductivity by 132.4 %, with potential applications in textiles, coatings, and thermal sensors.

The second type of thermochromic material is non-dye-based, including vanadium dioxide (VO_2), the most common inorganic thermochromic pigment and the main choice for building applications [2]. VO_2 is valued for its ability to modulate optical properties, particularly in the infrared range, unlike organic materials, which change color by altering reflectance in the visible range. It undergoes a reversible phase transition at around 68 °C, which can be lowered to around 40 °C by doping with tungsten, improving the efficiency of thermal regulation without altering the visible appearance [22]. Most research into VO_2 has focused on its application in transparent building components, such as windows, to regulate transmittance in response to temperature changes [23,24].

Studies have demonstrated the potential of VO2 for energy savings. For instance, Giovannini et al. [25] reported that VO_2 applied to glass in office buildings reduced energy consumption by 3–10 %, increased natural light availability by 5–20 %, and reduced glare by up to 50 %. Similarly, Aburas et al. [26] found energy savings ranging from 7.1 % to 46.4 % depending on coating thickness and climate, with the thickest glass providing the highest savings (33.3–46.4 %) and minimal impact on lighting consumption. Using a heat transfer model, Khaled et al. [27] evaluated VO_2-coated thermochromic glass. They reported energy use intensity reductions of up to 6.3 kWh/m^2 in Toronto, with higher savings of 12 kWh/m^2 in warmer climates. Fahland et al. [28] developed a VO_2 coating on flexible glass that achieved 50 % light transmittance and 9.6 % solar modulation. Khaled et al. found that VO_2 glass was more efficient than ligand exchange thermochromics (LET) in the cold climate of Toronto due to its low solar transmittance and high infrared reflectance [29].

Despite its potential for energy savings, VO_2 also has limitations. Wu et al. [30] reviewed thermochromic and electrochromic smart windows, emphasizing the role of inorganic pigments in regulating heat and light transmission to reduce heating and cooling demands. However, due to challenges related to durability, cost, and occupant thermal comfort, further research is needed to enhance dynamic performance and facilitate the integration of these materials into large-scale building designs. Similarly, Jiang et al. [31] discussed VO_2 coatings, highlighting their potential to reduce energy consumption by regulating heat gain through windows. However, despite advancements in nanostructuring and doping techniques, high transition temperatures and low visible light transmittance remain drawbacks.

As shown above, most of the research on inorganic thermochromic pigments has focused on the application of VO_2 to glass coatings, while its use on opaque building surfaces has been limited to date [32,33]. However, some studies have explored this application. Sirvent et al. [34] investigated its application to cement-based materials, in which VO_2 improved reflectance modulation, and the thermochromic properties remained stable during durability tests. More recently, Perez et al. [35] incorporated VO_2 thermochromic particles into cement paste and found that 9 % VO_2 delayed initial hydration, increased mechanical strength, and improved pore structure after 28 days, with noticeable thermochromic behavior in NIR reflectance.

Researchers have also incorporated SiO_2 and TiO_2 particles to improve the long-term performance of inorganic thermochromic pigments. Top et al. [36] developed VO_2/TiO_2 bilayer films that enhanced visible transmission by 30 % and infrared modulation by 20 %. Additionally, the TiO_2 layer protected the VO_2 from oxidation and provided superhydrophobicity, improving the overall performance and durability of the material. Pi et al. [37] created a thermochromic, hydrophobic, self-cleaning VO_2-SiO_2 film that improved solar protection (ΔT_{sol} from 9.9 % to 15.4 %) and light transmission (47.9 %–51.5 %), showing promise for energy-efficient buildings. Liu et al. [38] developed a multifunctional VO_2/PDMS film with anti-icing, self-cleaning, and durability properties, demonstrating the potential for energy-efficient applications. Khaled et al. [39] optimized VO_2 coatings with a 41 °C transition temperature and 4 °C hysteresis, suggesting future improvements with SiO_2 coatings and photothermal nanoparticles.

To assess the long-term performance of thermochromic materials, several studies have used different aging methods to evaluate the effect of weathering on their optical behavior in building applications. Soudian et al. [40] investigated the degradation of the solar reflectance of façade plasters containing thermochromic pigments through UV aging tests according to ASTM G154-16, simulating two years of natural exposure in seven days. Liu et al. [5] developed a superhydrophobic thermochromic coating and evaluated its UV resistance through 200 h of aging using 313 nm lamps, measuring wettability at regular intervals. *Xi* et al. [41] investigated LDPE-based thermochromic cooling materials by performing thermal aging at 80 °C for 48 h and repeated thermal cycling between 0 and 80 °C. Badino et al. [15] evaluated the durability of leuco dye-based thermochromic coatings under real outdoor summer conditions in Turin, Italy. Wang et al. [42] and Xu et al. [43] tested VO_2-based composite films under accelerated conditions of 100 °C and 50 %

relative humidity for 744 h and estimated the lifetime using the Hallberg-Peck model. Liu et al. [44] proposed a lead-safe thermochromic perovskite smart window and conducted a 45-day humidity aging test at approximately 60 % RH. Finally, Sun et al. [45] developed a thermochromic porous film and evaluated its reflectivity stability after 100 UV thermal cycles and its self-cleaning ability through simulated dust exposure.

These studies highlighted the energy-saving potential of both organic microencapsulated and inorganic pigments and identified key limitations to address. In summary, whereas thermochromic materials show great potential for enhancing building energy performance, the durability and cost optimization challenges remain. To mitigate such issues, incorporating SiO_2 and TiO_2 improved the durability and functionality of thermochromic coatings. These oxides contribute to better thermal regulation and mechanical stability while imparting self-cleaning and hydrophobic properties. Whereas SiO_2 is widely recognized for its chemical stability, water resistance, and inertness [46], TiO_2, on the other hand, exhibits strong photocatalytic activity due to its two main crystalline phases: rutile and anatase [47]. The TiO_2-P25 formulation, composed of approximately 75 % anatase and 25 % rutile, is particularly effective in combining high photocatalytic efficiency with long-term durability [48].

Beyond building applications, Papac et al. [49] studied the degradation of memantine, a persistent drug, using advanced oxidation processes. Their findings showed that the UV-A/TiO_2 system completely degraded memantine under optimized conditions, highlighting TiO_2-P25's photocatalytic potential. While focused on water treatment, the study reinforces TiO_2's relevance for self-cleaning coatings on sun-exposed surfaces. It identifies hydroxyl radicals as the primary reactive species, offering insights for developing more efficient photocatalytic materials. Other studies provide indirect insights for building applications. For example, humic substances from olive waste have been used in solar-assisted photo-Fenton processes, without TiO_2, demonstrating alternative degradation pathways under solar irradiation that could inspire hybrid solutions [50]. In addition, TiO_2 is widely used in dye-sensitized solar cells, which are being explored for energy-generating facades [51–53]. While primarily focused on energy generation, these studies highlight the material's versatility in architectural contexts.

Based on the above, this paper takes an experimental approach, combining the formulation and detailed laboratory characterization of thermochromic coatings and their components, to address two key challenges: the limited durability of organic thermochromic pigments and the lack of research on applying thermochromic materials to opaque surfaces, especially inorganic pigments. To address these issues, two coatings were developed, one with a microencapsulated organic thermochromic pigment (TC) and another with an inorganic thermochromic pigment (VO_2 doped with tungsten). Both were produced using the same formulation, combining an aqueous dispersion of colloidal silica (SiO_2) with titanium dioxide (TiO_2-rutile) for application on roof tiles. A key innovation is the addition of a protective layer of P25 titanium dioxide (TiO_2-P25) mixed with SiO_2 to increase durability and self-cleaning properties [46–48,54–56]. TiO_2-P25 consists of 25 wt% anatase, which provides photocatalytic self-cleaning and pollutant degradation under UV light [39]; the remaining 75 wt% of rutile stabilizes the system. SiO_2 further strengthens and extends the lifetime of the thermochromic coatings [54,55]. This approach is intended to enhance long-term performance and improve building energy efficiency by dynamically responding to temperature changes, potentially reducing the need for artificial air conditioning, CO_2 emissions, and the urban heat island effect. The following sections detail the coating's preparation, characterization, and performance analysis.

2. Materials and methods

2.1. Substracts preparation

Ceramic and fiber cement tiles were selected as substrates because of their widespread use in construction. Thirty-six samples were prepared for each substrate, resulting in 72 samples (6 samples × 6 coatings = 36 for each substrate). Thus, all tests were performed with six replicates per coating, which minimized the effect of single-sample variability and improved the statistical reliability of the results. The results shown in Section 3 represent the arithmetic average of 6 samples tested. This methodology ensured the reproducibility of the data obtained during the experimental characterization and allowed a proper evaluation of the experimental uncertainty.

The ceramic samples were prepared by uniaxial pressing (5 MPa, 60 s) of a clay-sand mixture (supplied by a tile manufacturer) into 2 × 7 × 0.5 cm prisms, followed by thermal treatment at 970 °C for 40 min in an electric furnace. This production method inherently introduces variability due to the granular nature of the raw materials and the compaction process. On the other hand, the fiber cement substrates were extracted from commercial flat sheets using a diamond-coated rotary saw, following the same dimensions as the ceramic samples.

A selection process based on flexural modulus was used to reduce these variations and ensure uniformity among the samples. Flexural modulus is a property that is highly sensitive to microstructural features such as porosity. For this selection, the dimensions (length, L; width, W; thickness, T, in cm) and mass (M, in g) of each sample were measured to calculate the apparent geometric density (AD, in g/cm3) as shown in Equation (1):

$$AD = M / (L \times W \times T) \quad (1)$$

The flexural modulus (E, in GPa) was then determined using the impulse vibration excitation technique (Sonelastic, ATCP, Brazil) according to ASTM E1876-01 [57]. Since the modulus calculation requires the apparent density as an input, both properties were measured for each sample. Initially, a larger batch of samples was prepared and tested. The arithmetic mean and standard deviation of the flexural modulus were calculated and the results were ranked in ascending order. Only specimens with modulus values within the mean ± 3 standard deviations were selected. This filtering process eliminated outliers and ensured that only mechanically consistent specimens were included in the final set of 36 specimens per substrate.

2.2. Coating development

This research employed the following raw materials: microencapsulated organic thermochromic pigments (TC: ChromaZone, TMC Hallcrest, GB), inorganic thermochromic elements (VO_2-W: Nano Vanadium Dioxide Doped with Tungsten, Hongwu International Group Ltd., CN), reflecting pigment (TiO_2: rutile titanium oxide, Labsynth, BR), photocatalytic titania (TiO_2-P25: Aeroxide TiO_2 P25, Evonik, DE), binder and stabilizing agent (SiO_2: aqueous dispersion of silanized colloidal silica, Levasil FX-401, 40 wt% of solids, Nouryon AB, Sweden), and a waterproof resin (multi-purpose "Acqua" resin, Hydronorth, BR).

The thermochromic transition temperature (TT) of the thermochromic pigments used in this research was determined by differential scanning calorimetry (DSC, DSC-6000, PerkinElmer). The method used consisted of two heating stages and an intermediate cooling stage. Firstly, the samples were heated from −20 °C up to 120 °C at a heating rate of 10 °C/min and cooled from 120 °C to −20 °C at a heating rate of 10 °C/min. The gas used for this experiment was high-purity N_2 under a 50 mL/min flow rate.

The solar reflectance of thermochromic pigments (TC, VO_2-W) and titania (TiO_2, P25) was measured using an Agilent CARY 5000 UV–VIS–NIR spectrophotometer (Fig. 1a) equipped with a diffuse reflectance accessory (DRA) with a 110 mm integrating sphere to

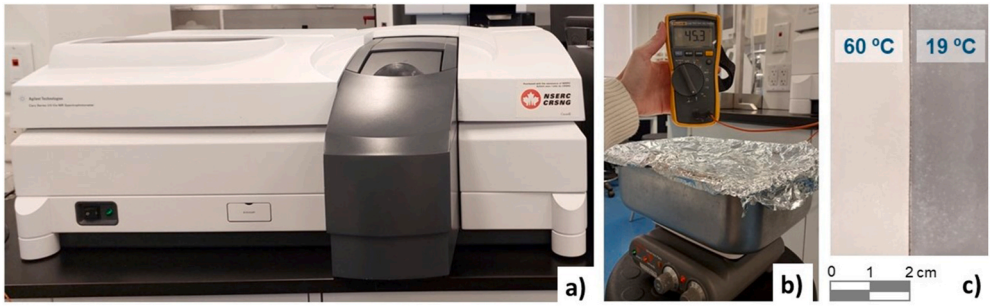

Fig. 1. a) Cary 5000; b) Temperature control; c) samples above and below TT.

capture the spectral reflectance over the 300–2500 nm range where solar energy is most concentrated [58]. A spectral correction was applied to accurately represent the material's behavior in real sunlight using the hemispherical spectral solar irradiance table from ASTM G173-23 [59].

The powders were first evaluated at room temperature (19 °C) to assess reflectance below the transition temperature. They were then heated on a hot plate (Corning, 4 × 5 Inch Top PC-220 Hot Plate/Stirrer, 120V/60Hz) to assess solar reflectance above the thermochromic transition (Fig. 1b). A K-type thermocouple connected to a Fluke 116 HVAC/R multimeter monitored the sample temperatures to ensure they remained at least 15 °C above the transition temperature, keeping the samples in the colorless phase throughout the spectrophotometer measurement (Fig. 1c).

The morphology and topography of the surfaces of all the materials used in this research were analyzed by scanning electron microscopy (FEG-SEM, Inspect-F50, FEI, Netherlands). Samples were previously coated with thin gold to improve their electrical conductivity and enhance the quality of the images.

The chemical composition and bonding characteristics of the microencapsulated organic thermochromic pigment (TC) were analyzed using a Cary 630 FTIR spectrometer (Agilent), operating in the ZnSe range from 5100 to 600 cm^{-1} with a resolution of $\leq$4 cm^{-1}. FTIR is particularly effective for identifying chemical bonds in polymers, but is less suitable for inorganic materials such as vanadium (VO_2-W), titania (TiO_2, TiO_2-P25), and colloidal silica (SiO_2), which have crystalline or amorphous structures that absorb little or no radiation in the mid-infrared region. Thus, only the organic TC was analyzed, identifying the polymers that comprise the shell and the thermochromic core for a detailed chemical characterization.

X-ray diffraction (XRD) was used to determine the crystalline phases of the inorganic pigment VO_2-W, providing insight into its crystal structure. Analyses were conducted using an XRD-6000 diffractometer (Shimadzu) with Cu-Kα radiation (λ = 1.54439 Å) in a 1-degree per minute scan rate. Their solid density was determined by helium pycnometry (Utrapyc-1200, Quantachrome Instruments, US).

Based on these characterizations, the thermochromic coatings were formulated with the proportions of each component adjusted to ensure adequate flow, good coverage, and easy application. Since colloidal silica (SiO_2) served as the coating base, each component was mixed with the SiO_2 dispersion to evaluate interactions and achieve a well-integrated, stable formulation (Fig. 2a). Widely used as a binder, colloidal SiO_2 consists of an aqueous suspension of spherical nanoparticles (20 nm average diameter) with a 40 wt% solid load. Through chemical processes or drying, these particles form a high-strength gel that binds and reinforces the coating [55].

Next, ternary combinations of colloidal silica (SiO_2), thermochromic pigments (TC or VO_2-W), and rutile titanium dioxide (TiO_2) were tested under the same conditions (Fig. 2b). Once stable suspensions were obtained, their application on ceramic and fiber cement roof tiles was evaluated. A foam roller (4 cm diameter × 15 cm length) provided the best results regarding layer homogeneity, ease of application, and overall effectiveness.

The most consistent formulation involved four layers: (1) a white primer to standardize the substrate; (2) the thermochromic coating in a SiO_2 matrix; (3) a layer of P25 mixed with a SiO_2-based matrix to enhance the long-term performance of the thermochromic pigment; and (4) a waterproof resin to seal and protect the system (Fig. 2c). Application intervals were 4 h for the primer and 1 h between the thermochromic and resin layers.

The samples were dried in a controlled environment at 25 °C (maintained by air conditioning) to provide proper colloidal silica gelation and complete coating consolidation (Fig. 2d). Uncoated samples and samples coated only with commercial white acrylic paint were used as controls to compare the thermochromic coatings with conventional solutions. In addition, three samples from each of the six paint groups were weighed layer by layer to ensure reproducibility. The data from these 36 samples were used to calculate the average weight of each

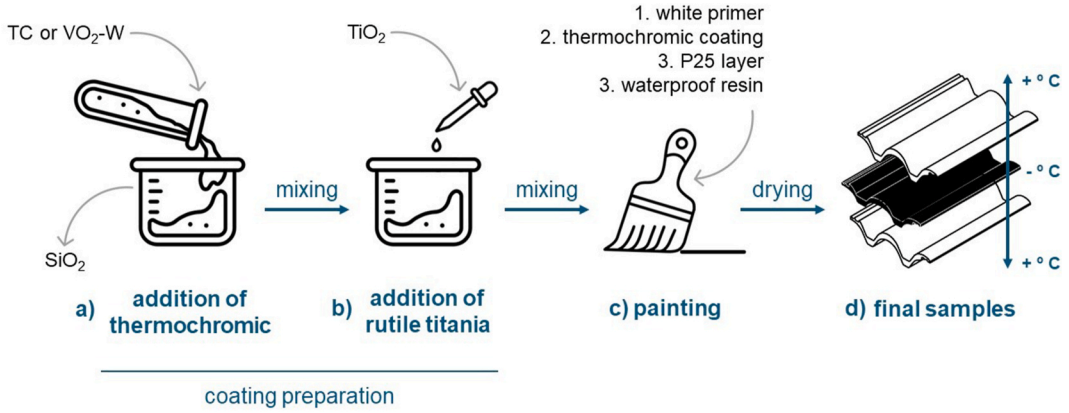

Fig. 2. Schematic diagram of the fabrication process of the thermochromic coating.

layer, indicating the paint yield and potential cost for large-scale production in the construction market.

2.3. Samples characterization

The coated samples were characterized for their optical (solar reflectance and thermal emissivity) and surface properties. Solar reflectance was first measured using the same spectrophotometer (Agilent, model CARY 5000 UV–VIS–NIR) and methodology described for the powders in section 2.2 [58,59]. Thermal emissivity was then evaluated following ASTM E1933-14 [60]. The standard recommends creating a temperature difference between the sample and the environment to ensure accurate measurements with an infrared camera (Fluke Ti450 PRO), improving contrast and focus. To achieve such a condition and measure both below and above the transition temperature of the thermochromic samples, a PolyScience immersion freeze-thaw bath was used to heat the samples to 60 °C. In contrast, a conventional refrigerator cooled them to approximately 10 °C.

Infrared thermography was performed using the non-contact method. The Fluke Ti450 PRO camera (7.5–14 μm spectral band, ±2 °C accuracy) was used, with black electrical tape ($\varepsilon = 0.96$) applied to the corner of the tiles as a reference material (Fig. 3). All tests were conducted in a controlled laboratory environment (21 °C). After heating the samples to 60 °C, they were immediately measured to ensure they remained above the transition temperature. The camera emissivity was adjusted based on the known emissivity of the tape, and the surface temperatures of both the tape and samples were recorded. Using SmartView software (Version 4.4), the sample surface temperature was calibrated to match that of the tape, which served as the reference due to its known emissivity value. After capturing infrared images of the heated samples, they were cooled to 10 °C in a conventional fridge, and the process was repeated.

The hydrophobicity of the coatings was analyzed using ASTM D7334-08 [61], which establishes procedures for measuring contact angles using water droplets as a reference liquid to evaluate surface wettability. Since hydrophobic agents such as SiO_2 and a commercial waterproofing resin were used, the coating could help protect surfaces from weathering and facilitate self-cleaning through rainwater action. Measurements were conducted using an Ossila Contact Angle Goniometer (range: 5°–180°, accuracy: ±1°) with associated software (v4.1.3.0), which calculates the contact angle between a water droplet and the substrate (Fig. 4). A surface is classified as hydrophilic when the contact angle is below 90°, indicating greater wettability, whereas angles above 90° denote hydrophobicity, meaning reduced water adhesion [61]. Since changes in solar reflectance due to sample heating do not affect hydrophobicity, all measurements were performed at room temperature (21 °C).

3. Results

3.1. Characterization of coating components

3.1.1. Differential scanning calorimetry (DSC)

The DSC results provided insight into the thermal behavior of the thermochromic samples, highlighting their phase transitions (Fig. 5). VO_2-W exhibited a well-defined endothermic peak at 46.89 °C, indicating a sharp and reversible phase transition with minimal thermal hysteresis. In contrast, TC showed a more complex response with major peaks at 39.88 °C and 66 °C (Table 1), probably due to its core-shell microstructure consisting of two polymers separated by an interfacial phase. TC also exhibited a more intense endothermic peak, requiring more energy for its phase transition, and a higher thermal hysteresis, indicating a more gradual phase change. However, DSC analysis confirmed its stable thermal profile at higher temperatures, indicating effective encapsulation of the thermochromic dye.

3.1.2. Solar reflectance

The organic thermochromic pigment (TC) showed a clear change in VIS reflectance, as its color visibly shifts above the transition temperature (Fig. 6). In contrast, the inorganic thermochromic pigment (VO_2-W) showed no significant change, an unexpected result that differs from Sirvent et al. [34], where VO_2 powder showed a clear NIR shift. One likely reason for this difference is the specific thermal and optical properties of VO_2. As an inorganic material, VO_2 has a more organized atomic structure, which allows heat to move more quickly through the material (higher thermal conductivity). In addition, VO_2 has a lower heat capacity than organic pigments, which means it does not hold heat either. Organic pigments, on the other hand, have more complex molecular structures that allow them to retain heat longer. For this reason, VO_2 may have cooled too quickly below its transition temperature during the spectrophotometric measurement, which could explain why no thermochromic behavior was detected. The rapid heat loss may have caused the material to miss the temperature range where the transition occurs. Other factors, such as particle size, crystallinity, or surface oxidation of VO_2 and insufficient tungsten doping, may also have contributed to the lack of thermochromic response.

TiO_2 and P25 performed as expected, both exhibiting high solar reflectance. However, despite its similar appearance to the naked eye,

Fig. 3. a) Thermal emissivity temperature control system; b) Black tape applied.

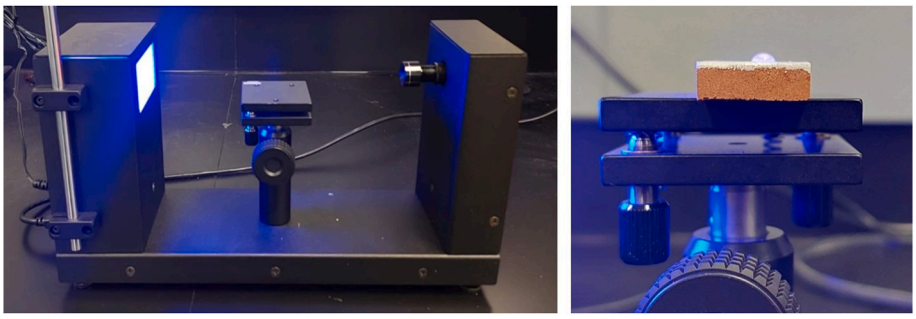

Fig. 4. a) Contact Angle Goniometer; b) Drop of water on VO_2-W sample surface.

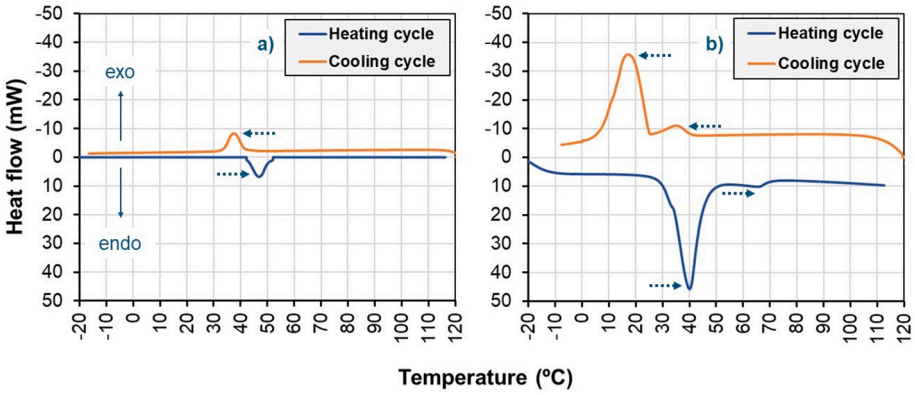

Fig. 5. DSC analysis for thermochromic pigments: a) inorganic (VO_2-W); b) organic (TC).

Table 1
Summary of DSC curve results.

Sample	Heating cycle		Cooling cycle	
	T_{endo1} (° C)	T_{endo2} (° C)	T_{exo1} (° C)	T_{exo2} (° C)
VO_2-W	46.89	–	37.61	–
TC	39.88	66.23	17.01	35.15

P25 had an even higher reflectance, reaching maximum values over most of the VIS spectrum (380–780 nm, highlighted in light gray). This can be attributed to its smaller particle size compared to rutile TiO_2, which improves light dispersion through better particle packing.

3.1.3. *Scanning electron microscope (SEM)*

The thermochromic pigments had the largest average particle size among all raw materials. VO_2-W (2–10 μm), exhibited significant size variation, which may facilitate its packing. However, its non-spherical shape and larger size limit its surface area and reduce its reactivity. In addition, a whisker-like carbon coating was observed around the VO_2-W particles, which likely protects the tungsten in the composite from oxidation (Fig. 7a). The organic pigment, TC (1–5 μm), is more homogeneous and has a larger surface area and higher reactivity due to its smaller size. The polymeric resin that encapsulates these particles ensures uniformity of size and shape while protecting the thermochromic pigments inside, preserving their properties over time (Fig. 7b).

TiO_2 rutile (0.1–0.3 μm) is a cost-effective white pigment widely used in paints for its optical properties, durability, and opacity, reducing the need for multiple coats [62]. It also improves the packing between thermochromic particles and colloidal silica (SiO_2), increasing mechanical strength and reducing water permeability (Fig. 7c). SiO_2 (0.08–0.1 μm), considered a nanomaterial due to its particle size below 0.1 μm [63], serves as a binder, keeping the film components integrated during drying until gel formation. Once formed, the coating fills the substrate pores, creating a hydrophobic barrier. This water-repellent

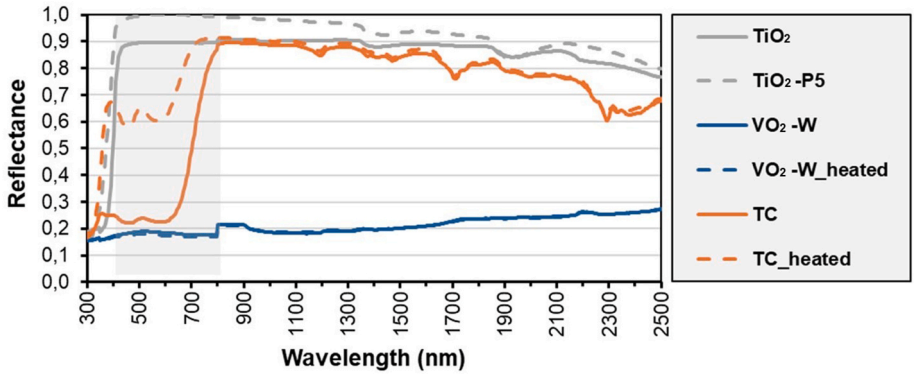

Fig. 6. Solar reflectance curve of the coating component powders.

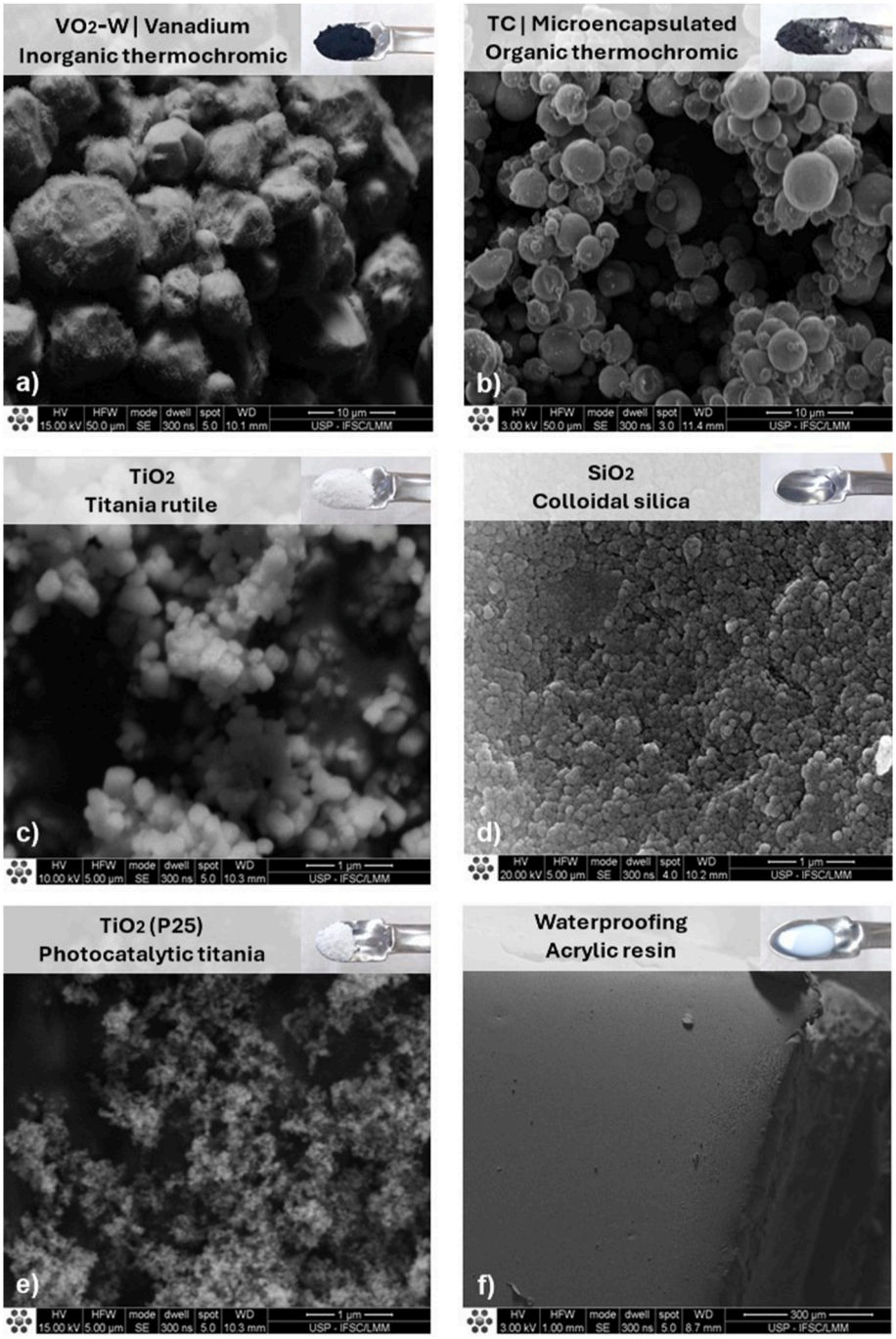

Fig. 7. SEM images of materials.

property stems from the surface modification of silica with organic functional groups, which enhance durability and reduce water permeability [54,64] (Fig. 7d). TiO_2-P25 (0.02–0.03 μm), also considered a nanomaterial, is the most reactive material in the film due to its high surface area and photocatalytic activity (Fig. 7e). Finally, for the waterproofing resin, although its primary particles were not clearly visualized by SEM, a sealing gel was observed after drying, confirming its role in protecting and finalizing the system (Fig. 7f).

3.1.4. Fourier transform infrared spectroscopy (FTIR)

The reversible color change of organic thermochromic pigments occurs as their molecular structure reorganizes with temperature. In the cooled state (below 37 °C), the N,N-dimethyl-ethanamine group ($(C_2H_5)2N^+$) enables the molecule to absorb light, resulting in darker colors. Upon heating, the resonant bonding of the aromatic rings shifts the carboxyl group into a carbonyl once the H^+ is released. The oxygen ring closing stabilizes the molecule, hindering its ability to absorb light, turning it into a whitish aspect [17].

FTIR analysis of the microcapsule shell (Fig. 8) was performed to understand the structural behavior of these thermochromic pigments. The results revealed the presence of melamine-formaldehyde, which plays a crucial role in the stability and functionality of the system. The main peak at 1500 cm^{-1} corresponds to aromatic ring deformations and triazine groups typical of melamine-based polymers. Peaks within 1400–1600 cm^{-1} confirm these structures, while those at 1200-1300 cm^{-1} indicate C-N bonds, characteristic of nitrogen-rich polymers. The 1000-1100 cm^{-1} band indicates C-O stretching in the cross-linked structure. The C-H stretching bands (2800-3000 cm^{-1}) suggest methyl

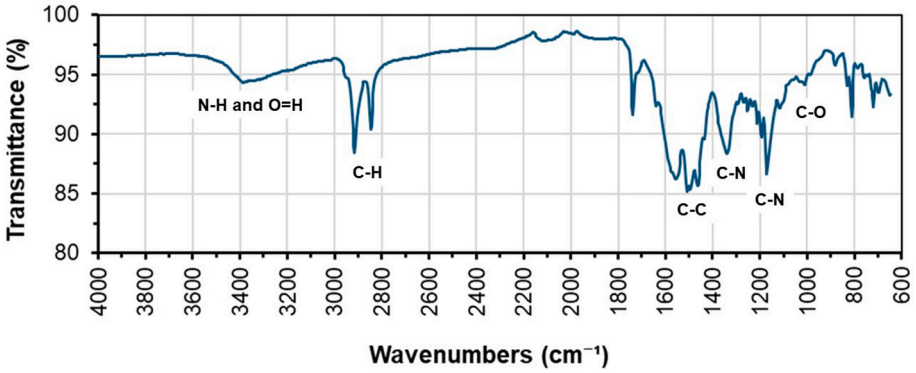

Fig. 8. TC FTIR curve.

or methylene groups, while the broadband at 3200-3600 cm^{-1} indicates residual N-H and O-H groups. These findings corroborate melamine-formaldehyde's thermal and chemical resistance, consistent with the observed stability of the thermochromic pigments during multiple heating and cooling cycles, as confirmed by DSC analysis (Fig. 5b).

3.1.5. X-ray diffraction (XRD)

As shown in Fig. 9, XRD analysis of VO_2-W confirms that the sample consists primarily of vanadium dioxide (VO_2) with a small fraction (1.6 wt%) of tungsten oxide (WO_3). The well-defined diffraction peaks indicate a crystalline material with VO_2 as the dominant phase. The low-intensity WO_3 peaks suggest that tungsten is likely to dope the VO_2 structure rather than form a separate phase. The main purpose of tungsten doping is to lower the phase transition temperature of VO_3 from 68 °C to around 40 °C, making the pigment more suitable for building envelope applications to improve thermal and energy efficiency [34].

3.2. Composition and application of coatings

As described in Section 2.2, four different layers were applied to each substrate. The composition of these layers is shown in Table 2, where the pigment percentages refer to the mass of the SiO_2 binder. This binder was critical in integrating the components during drying and ensuring gel formation. In addition to these compositions, two control groups were prepared for comparison. The first group consisted of samples coated only with a white primer and a hydrophobic resin applied to ceramic and fiber cement substrates, comparing dynamic thermochromic films and conventional static white coatings. The second group included raw ceramic and fiber cement samples with only the hydrophobic resin applied. Fig. 10 shows the appearance of all samples.

Table 2
Coatings formulation.

Layer	Coatings					
	Reference	White	VO_2-W	VO_2-W + P25	TC	TC + P25
1	Primer	–	Primer	Primer	Primer	Primer
2	–	–	Coating	Coating	Coating	Coating
	–	–	SiO_2	SiO_2	SiO_2	SiO_2
	–	–	10 % VO_2	10 % VO_2	7 % TC	7 % TC
	–	–	40 % TiO_2	40 % TiO_2	5 % TiO_2	5 % TiO_2
3	–	–	–	1 % P25	–	1 % P25
4	Resin	Resin	Resin	Resin	Resin	Resin

No significant visual differences were observed between the two substrates for the same coating. The organic thermochromic (TC) samples appeared gray due to TiO_2, which lightened the color compared to the pure thermochromic powder. The VO_2 samples, which contain large particles that settle easily, proved difficult to mix uniformly. In addition, these samples did not show a significant shift in the IR region, as it was initially expected. A lower amount of VO_2 was used to overcome this, resulting in a white finish, mainly due to the higher TiO_2 content.

The addition of P25 had different effects on the VO_2 and TC-containing samples. It brightened the surfaces of both VO_2 substrates while causing an irregular, stained finish on the TC samples, especially

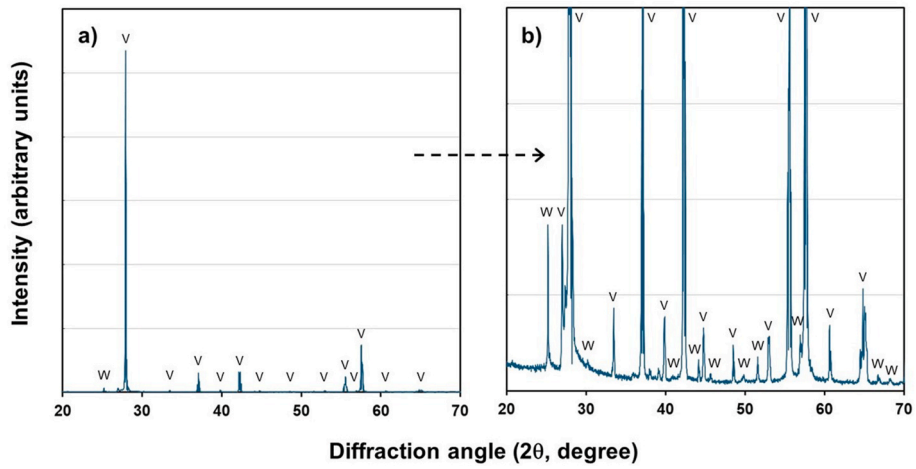

Fig. 9. X-ray diffraction pattern for vanadium dioxide sample: a) full curve; b) higher magnification. List of symbols (PDF file, wt%): V = VO_2 (96-900-9090; 98.4 wt %); W = WO_3 (96-152-1535, 1.6 wt%).

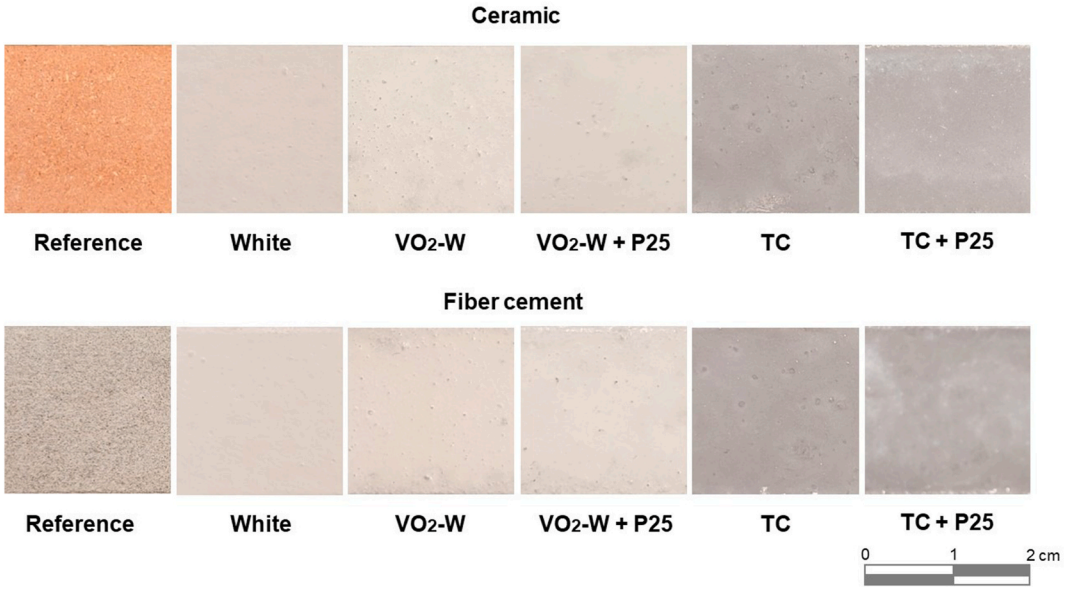

Fig. 10. Finished samples.

on the fiber cement tiles due to their rough surface. All images were taken at 19 °C, with the adaptive samples below their transition temperature. Noticeable color changes occurred only on the TC samples.

Table 3 shows the average weight per unit area of the samples. Due to their high solid density, the layers with the highest mass for both substrates were those containing VO_2-W, while the final hydrophobic resin layer with the lowest solid content had the lowest mass. Notably, there was a significant mass difference between the organic TC layer and the inorganic VO_2-W layer for the same substrate. Generally, the mass of VO_2-W was twice that of TC for ceramic and fiber cement samples.

The greatest difference occurred in the white primer (first layer), due to the fiber cement substrate's higher porosity than the ceramic one. In contrast, the last two layers, P25 and the waterproof resin, had higher basis weights on the ceramic samples. These variations can be attributed not only to the permeability of the substrate but also to the particle characteristics in each layer and the natural variability of the manual application method. Ceramic tiles offer a slightly better cost/benefit ratio because they retain less paint than fiber cement, resulting in lower material consumption.

3.3. Samples characterization

3.3.1. Solar reflectance

As shown in Table 4, the solar reflectance of the analyzed coatings is similar regardless of the substrate, indicating that the coating has a greater influence than the substrate. These results were expected because solar reflectance is a material surface property. However, although the substrate is a secondary influence, coatings tend to be more reflective when applied over ceramic substrates than fiber cement ones, as shown in Table 5. The only exception was the VO_2-W coating, which showed higher reflectance on fiber cement below and above the transition temperature. This suggests that ceramic substrates enhance NIR reflectance (0.731 vs. 0.440), which increases overall reflectance. Factors such as color, composition, and thermal properties likely contribute. A similar pattern was observed for white-coated samples, where ceramic substrates showed higher reflectance in all spectral regions.

Table 6 shows the percentage differences in reflectance measured for the thermochromic samples above and below the transition temperature. The TC-containing coatings exhibited significant changes in solar reflectance, particularly in the visible (VIS) spectrum (ranging from 72 to 95 %), with a total reflectance variation between 29 and 39 % for both substrates. All spectral regions became more reflective when heated above the transition temperature, with the near infrared (NIR) region being the least affected.

Although the total solar reflectance (T) was higher for ceramic substrates (TC: 0.596; TC-P25: 0.628) than for fiber cement (TC: 0.566; TC-P25: 0.606), the relative increase in reflectance with temperature was more pronounced for fiber cement - 8 % higher for TC coatings and 9 % higher for TC-P25 coatings compared to ceramic. This suggests that fiber cement enhances the thermochromic effect, likely due to differences in material properties. Adding P25 increased the VIS reflectance in the darker phase (below the transition temperature) due to its white pigmentation. However, once the coatings turned white on heating, P25 had little effect because the coatings were already highly reflective. Hence, the reflectance curves for coatings with and without P25 were nearly identical after heating.

For coatings containing inorganic thermochromic pigments (VO_2-W), an increase in solar reflectance, especially in the NIR region, was expected upon heating. However, the observed changes were minimal, with the total reflectance varying by less than 2 % for all samples. Surprisingly, the total solar reflectance slightly decreased instead of increasing, meaning that the coatings became less reflective upon heating. This effect contradicted previous studies that reported higher solar reflectance for VO_2-based samples at elevated temperatures, especially in the NIR [34,35]. However, it is consistent with the

Table 3
Basis weights.

Substracts	Average basis weight per layer (g/cm^2)				
	Primer	VO_2-W	TC	P25	Resin
Ceramic	0.0024	0.0257	0.0100	0.0044	0.0006
Fiber cement	0.0035	0.0271	0.0136	0.0039	0.0001
F/C (%)	48 %	6 %	36 %	−11 %	−88 %

Table 4
Solar reflectance (ρ) measurement for the UV–VIS–NIR bands.

Samples	Ceramic (C)							
	T	UV	VIS	NIR	T heated	UV heated	VIS heated	NIR heated
Reference	0.524	0.155	0.383	0.731	–	–	–	–
White	0.882	0.155	0.911	0.898	–	–	–	–
VO_2-W	0.792	0.145	0.868	0.743	0.790	0.143	0.863	0.744
VO_2-W + P25	0.827	0.207	0.895	0.787	0.815	0.208	0.878	0.778
TC	0.596	0.151	0.404	0.875	0.814	0.17	0.791	0.891
TC + P25	0.629	0.211	0.462	0.874	0.817	0.219	0.796	0.887
Samples	**Fiber cement (F)**							
	T	**UV**	**VIS**	**NIR**	**T heated**	**UV heated**	**VIS heated**	**NIR heated**
Reference	0.407	0.280	0.389	0.440	–	–	–	–
White	0.857	0.154	0.894	0.862	–	–	–	–
VO_2-W	0.824	0.153	0.891	0.788	0.812	0.149	0.878	0.775
VO_2-W + P25	0.829	0.228	0.899	0.783	0.814	0.22	0.876	0.779
TC	0.567	0.149	0.399	0.813	0.791	0.164	0.778	0.853
TC + P25	0.607	0.205	0.448	0.84	0.804	0.215	0.792	0.862

Table 5
Solar reflectance (ρ) percentage difference between F and C substrates.

Samples	Fiber cement (F)/Ceramic (C)							
	T	UV	VIS	NIR	T heated	UV heated	VIS heated	NIR heated
Reference	−22.3 %	80.6 %	1.3 %	−39.8 %	–	–	–	–
White	−2.8 %	−1.3 %	−2.0 %	−4.0 %	–	–	–	–
VO_2-W	4.0 %	5.5 %	2.6 %	6.1 %	2.8 %	4.2 %	1.7 %	4.2 %
VO_2-W + P25	0.2 %	10.1 %	0.4 %	−0.5 %	−0.1 %	5.8 %	−0.2 %	0.1 %
TC	−4.9 %	−1.3 %	−1.2 %	−7.1 %	−2.8 %	−3.5 %	−1.6 %	−4.3 %
TC + P25	−3.5 %	−2.8 %	−3.0 %	−3.9 %	−1.6 %	−1.8 %	−0.5 %	−2.8 %

Table 6
Percentage change in solar reflectance (ρ) for thermochromic paints after heating.

Samples	Ceramic (C)			
	Δ% T	Δ% UV	Δ% VIS	Δ% NIR
VO_2-W	−0.25 %	−1.38 %	−0.58 %	0.13 %
VO_2-W + P25	−1.45 %	0.48 %	−1.90 %	−1.14 %
TC	36.58 %	12.58 %	95.79 %	1.83 %
TC + P25	29.89 %	3.79 %	72.29 %	1.49 %
Samples	**Fiber cement (F)**			
	Δ% T	**Δ% UV**	**Δ% VIS**	**Δ% NIR**
VO_2-W	−1.46 %	−2.61 %	−1.46 %	−1.65 %
VO_2-W + P25	−1.81 %	−3.51 %	−2.56 %	−0.51 %
TC	39.51 %	10.07 %	94.99 %	4.92 %
TC + P25	32.45 %	4.88 %	76.79 %	2.62 %

characterization of pure VO_2-W pigments presented in Section 3.1.2, where minimal reflectance variation was observed. In addition, P25 did not affect on solar reflectance in any spectral region, regardless of temperature.

Figs. 11 and 12 show the reflectance curves for all coatings applied to ceramic and fiber cement substrates. The results show that the coating has similar reflectance patterns and values on both substrates. The effect of heating on reflectance becomes more apparent in these curves over the entire solar spectrum. Coatings containing VO_2-W showed minimal changes when heated, while those with TC pigments showed a significant shift, especially in the visible region, shaded in light gray in the graphs (380–780 nm).

The underperformance of the VO_2-W coating on ceramic and fiber cement tiles may be related to the limited exposure of vanadium atoms to infrared radiation. In glass, the parent material ($SiO_2 + Na_2O + CaO$) forms an amorphous structure that prevents crystallization and allows VO_2 to be uniformly distributed. This uniform distribution potentially leads to greater exposure of the vanadium atoms to infrared radiation, which enhances the thermochromic effect. In contrast, when applied by coating to opaque surfaces, the vanadium atoms within the particles may be less exposed to infrared radiation, reducing their contribution to the thermochromic behavior. As a result, the thermochromic efficiency per vanadium atom could be lower than in glass. To improve performance, optimizing the distribution of vanadium atoms or increasing tungsten doping could help improve infrared exposure and enhance thermochromic response.

3.3.2. *Thermal emissivity*

Fig. 13 shows the thermal emissivity values of the samples measured under cooled (10 °C) and heated (60 °C) conditions. To evaluate the influence of the type of substrate, samples with the same coating were placed side by side in the graph. The results showed a total range of 0.88–0.97, indicating high emissivity for all samples, with the reference ones showing the highest values. P25-containing samples resulted in more stable emissivity measurements, with minimal variation between cooled and heated conditions. In contrast, coatings without P25, particularly on ceramic substrates, showed the greatest variation when measured above and below the transition temperature. Unlike the solar reflectance results, thermal emissivity was largely unaffected by substrate or coating type, remaining consistent across samples.

3.3.3. *Hydrophobicity*

Fig. 14 shows that, due to their high porosity and permeability, the reference samples without the waterproofing resin absorbed the water drop immediately, making contact angle measurements difficult. However, waterproofing resin significantly increased their hydrophobicity, especially for the fiber cement samples.

A surface is hydrophobic if the contact angle exceeds 90° [61]. As shown in Table 7, only the fiber cement sample with the waterproofing resin reached this threshold. The thermochromic and conventional white coatings on the ceramic substrate improved the hydrophobicity compared to the resin-only reference. However, all painted samples on the fiber cement substrate had lower contact angles than the resin-only reference. This difference is likely due to the resin providing better coverage on the fiber cement, creating a more impervious surface. In

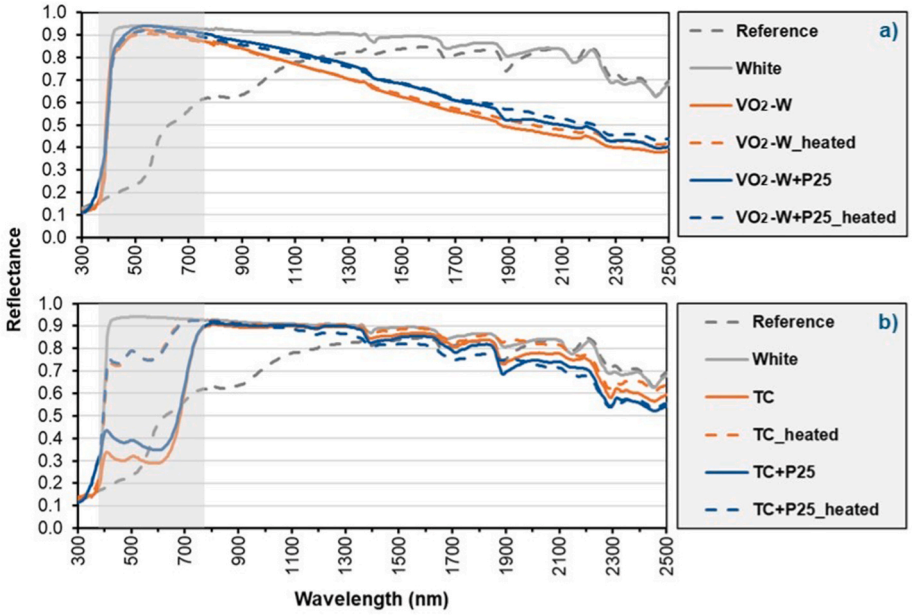

Fig. 11. Reflectance of ceramic substrates: a) VO_2-containing, b) TC-containing.

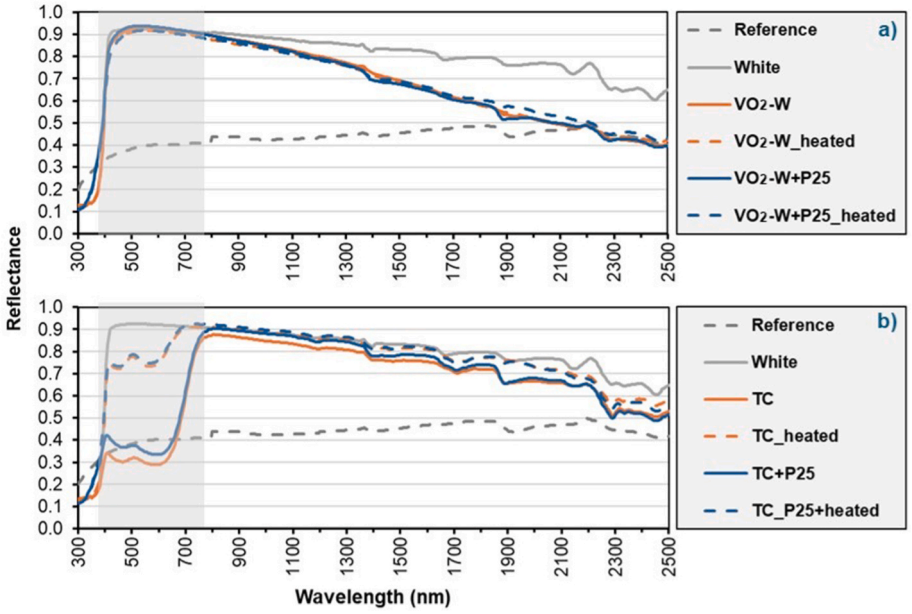

Fig. 12. Reflectance of fiber cement substrates: a) VO_2-containning, b) TC-containing.

contrast, the firing process of the ceramic substrate resulted in the efflorescence of molten salts during the sintering process, which hindered the paint and resin adhesion and caused coating imperfections [65].

Although the coatings did not achieve true hydrophobicity, they significantly improved the surface resistance to water absorption compared to uncoated ones. All contact angles were greater than 70°, indicating moderate hydrophobicity and resistance to wetting, but not the high repellency of superhydrophobic surfaces such as those described in other works [37,38].

4. Discussion

To assess the effect of P25 on the samples long-term performance, an accelerated ageing test was carried out by ASTM D7897-18 [66], simulating three years of natural exposure. The samples were exposed to alternating cycles of UV light, humidity, and controlled temperature in a QUV weathering chamber. They were then sprayed with an aqueous mixture designed to mimic average US environmental conditions before undergoing another exposure cycle. This methodology was specifically designed to assess the impact of P25 on the long-term durability of the developed samples.

Table 8 shows that accelerated aging was more pronounced in ceramic than fiber cement samples. The ceramic samples showed a 5.5 % reduction in solar reflectance, indicating a darkening of the surface, primarily due to the deposition of particulate matter during the soiling test. In contrast, the fiber cement samples showed less than 1 % variation in total solar reflectance with a slight increase, indicating a brightening of the surface, likely due to fading from UV exposure.

Both white-coated samples, whether with dynamic vanadium

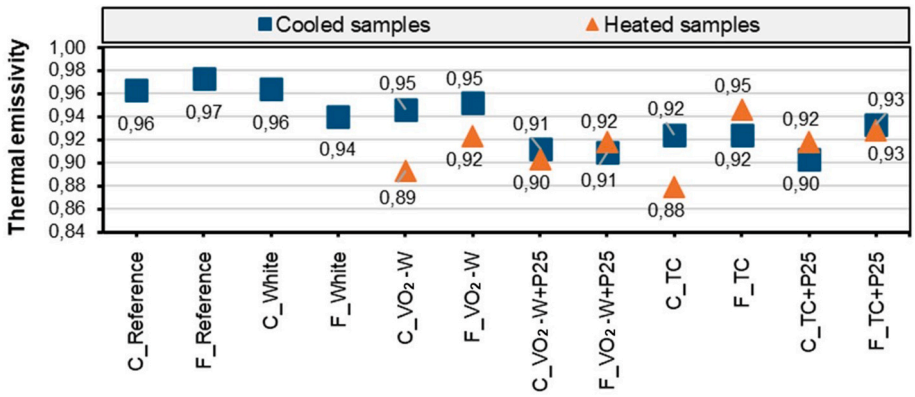

Fig. 13. Thermal emissivity variation.

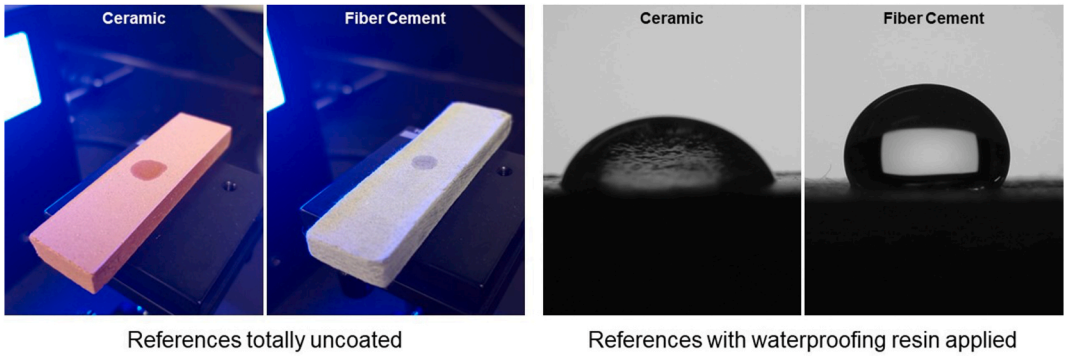

Fig. 14. Hydrophobicity Improvement for reference samples.

Table 7
Contact angle measurement.

Sample	Ceramic (°)	Fiber cement (°)
Reference	63.40	106.54
White	77.32	71.82
VO_2-W	78.03	77.84
VO_2-W + P25	80.44	74.97
TC	82.86	78.19
TC + P25	80.28	71.60

Table 8
Effect of accelerated aging test on solar reflectance (ρ).

Samples	Ceramic					
	ρ Initial	ρ Initial heated	ρ Aged	ρ Aged heated	ρ Δ%	ρ Δ% heated
Reference	0.524	–	0.495	–	−5.5 %	–
White	0.882	–	0.828	–	−6.1 %	–
VO_2-W	0.792	0.790	0.740	0.725	−6.6 %	−8.2 %
VO_2-W + P25	0.827	0.815	0.747	0.740	−9.7 %	−9.2 %
TC	0.596	0.814	0.686	0.733	15.1 %	−10.0 %
TC + P25	0.629	0.817	0.671	0.757	6.7 %	−7.3 %
Samples	**Fiber cement**					
	ρ Initial	**ρ Initial heated**	**ρ Aged**	**ρ Aged heated**	**ρ Δ%**	**ρ Δ% heated**
Reference	0.407	–	0.410	–	0.7 %	–
White	0.857	–	0.800	–	−6.7 %	–
VO_2-W	0.824	0.812	0.731	0.735	−11.3 %	−9.5 %
VO_2-W + P25	0.829	0.814	0.718	0.718	−13.4 %	−11.8 %
TC	0.567	0.791	0.642	0.703	13.2 %	−11.1 %
TC + P25	0.607	0.804	0.64	0.756	5.4 %	−6.0 %

dioxide (VO_2) or static conventional white coatings, showed a significant decrease in solar reflectance compared to their initial unaged state. This decrease in reflectance was observed for ceramic and fiber cement samples, which is expected since white and reflective surfaces are particularly susceptible to weathering, mainly due to particulate accumulation [67]. Contrary to expectations, the photocatalytic effect typically associated with the degradation of organic compounds and self-cleaning under simulated rain was not observed in the inorganic VO_2-W + P25 samples. Instead, the presence of P25 resulted in a more significant degradation of solar reflectance, which can be attributed to the final lighter color of the coating, suggesting that the VO_2-containing paints behaved similarly to static conventional white surfaces.

However, when applied to the TC-containing samples, the results showed that P25 effectively protected the dye pigments from UV degradation. On average, the TC samples with P25 degraded 57 % less in the below-transition-temperature phase and 37 % less in the above-transition-temperature phase than the TC samples without the P25 layer (Table 8). While P25 is typically evaluated for its photocatalytic activity in degrading organic compounds under UV or visible light, initial concerns about potential damage to the organic thermochromic microcapsules were not supported. Rather than deteriorating the dye, P25 helped to preserve its color, as shown in Fig. 15. Areas of higher P25 accumulation, often due to uneven application, provided the greatest protection to the thermochromic pigment after the accelerated aging test.

Although P25 did not demonstrate self-cleaning performance for the VO_2 samples, it played a significant protective role for the microencapsulated thermochromic pigment. P25 may have acted as a UV filter, absorbing radiation and preventing damage to the pigment chemical structure. In addition, P25 may have enhanced the microcapsule protective layer, making it more resistant to environmental changes, reducing oxidation, and minimizing degradation of the

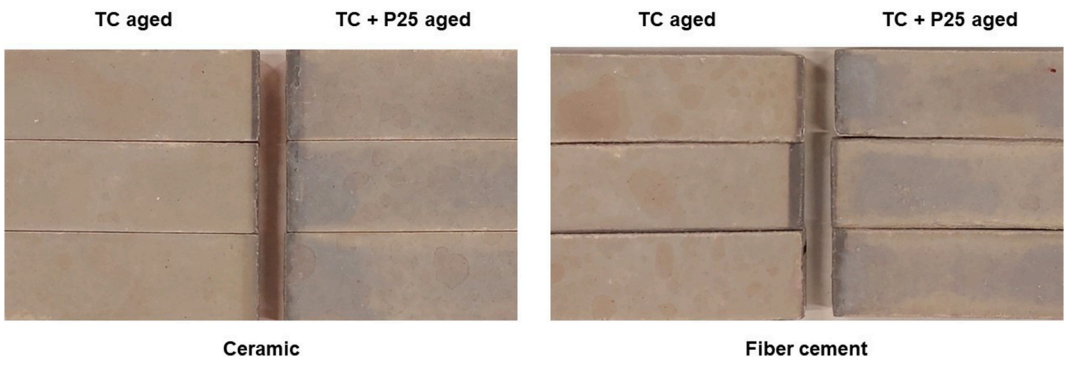

Fig. 15. Aging of TC samples, with and without P25, at room temperature.

compounds responsible for the color change. This helped to reduce weathering and prevent photochemical degradation.

5. Conclusions

The coatings developed in this study demonstrated stability across all components, with strong adhesion to the substrates and between the applied layers. These results confirm the feasibility of formulating a paint that integrates thermochromic pigments with colloidal silica, rutile titanium dioxide, and photocatalytic titanium dioxide.

The most significant result was the high performance of the organic thermochromic coating containing microencapsulated pigments, which exhibited a marked and reversible variation in solar reflectance in response to changes in surface temperature. This dynamic optical behavior highlights the material's potential for reducing cooling energy demands and enhancing thermal regulation in buildings. While further investigation is required to evaluate this effect in real-world conditions, the findings suggest that this formulation may contribute to energy efficiency strategies in the built environment.

In contrast, the inorganic vanadium-based thermochromic paint did not display any notable spectral response to temperature variation, indicating static behavior and an absence of the expected thermochromic functionality. Given its higher production complexity and cost, this formulation proved less effective than conventional white paints, which remain a more economical alternative for reflective coatings.

All tested coatings exhibited similarly high thermal emissivity values (above 0.87), suggesting that emissivity was not a distinguishing parameter for evaluating the coatings' thermal performance. However, the coatings also contributed to increased surface hydrophobicity, as demonstrated by contact angle measurements, which is beneficial for maintaining long-term reflectance and minimizing soiling effects.

This research's novelty and key contribution lie in demonstrating the protective role of the P25 titanium dioxide layer in enhancing the durability of organic thermochromic coatings. The P25 layer effectively acted as a UV barrier, stabilizing the microcapsules and mitigating photochemical and thermal degradation. This finding addresses one of the main challenges reported in the literature, the limited longevity of organic thermochromic systems under environmental exposure. Although further optimization is necessary, particularly regarding application uniformity and UV shielding, the results validate the strategy of combining organic thermochromic pigments with P25 to improve long-term performance.

In summary, this study's outcomes contributed to the ongoing development of adaptive coatings for opaque building surfaces. While additional improvements and long-term field evaluations are necessary, the findings reinforce the relevance of organic thermochromic pigments, especially when supported by photocatalytic additives such as P25, as a promising foundation for the advancement of next-generation smart coatings for architectural applications.

CRediT authorship contribution statement

Ana Carolina Hidalgo-Araujo: Methodology, Investigation. **Rafael Salomão:** Project administration, Methodology, Investigation. **Umberto Berardi:** Investigation, Formal analysis, Data curation. **Kelen Almeida Dornelles:** Project administration, Methodology.

Declaration of competing interest

The authors declare that they have no known competing financial interests or personal relationships that could have appeared to influence the work reported in this paper.

Acknowledgments

The authors thank the Brazilian Research Foundation FAPESP (Grants 2010/19274-5, 2022/14074-5, 2022/03655-7, 2024/00850-9 and 2024/10060-5), HERA (Holistic Energy Recovery Agent tool for sustainable urban clusters, PRIN 2022), and NETPLUS (Neighborhood Energy Transition: towards Positive energy balance and carbon neutral districts, PRIN PNRR) for supporting this work. They also thank Nouryon Latin America (Brazil) and AB (Sweden) for supplying SiO_2.

Data availability

Data will be made available on request.

References

[1] IPCC, Climate Change 2022: Impacts, Adaptation and Vulnerability: Sixth Assessment Report of the Intergovernmental Panel on Climate Change, Intergovernmental Panel on Climate Change, 2022.
[2] M. Santamouris, G.Y. Yun, Recent development and research priorities on cool and super cool materials to mitigate urban heat island, Renew. Energy 161 (2020) 792–807, https://doi.org/10.1016/j.renene.2020.07.109.
[3] S. Garshasbi, M. Santamouris, Using advanced thermochromic technologies in the built environment: recent development and potential to decrease energy consumption and fight urban overheating, Sol. Energy Mater. Sol. Cell. 191 (2019) 21–32, https://doi.org/10.1016/j.solmat.2018.10.023.
[4] C. Fabiani, A.L. Pisello, Passive cooling by means of adaptive cool materials, in: F. Pacheco-Torgal, L. Czarnecki, A.L. Pisello, L.F. Cabeza, C.-G. Granqvist (Eds.), Eco-efficient Materials for Reducing Cooling Needs in Buildings and Construction, Woodhead Publishing, 2021, pp. 439–457, https://doi.org/10.1016/B978-0-12-820791-8.00018-3.
[5] H. Liu, T. Jiang, F. Wang, W. Ou, J. Li, Thermochromic superhydrophobic coatings for building energy conservation, Energy Build. 251 (2021) 111374, https://doi.org/10.1016/j.enbuild.2021.111374.
[6] A. Hakami, S.S. Srinivasan, P.K. Biswas, Review on thermochromic materials: development, characterization, and applications, J. Coating Technol. Res. 19 (2022) 377–402, https://doi.org/10.1007/s11998-021-00558-x.
[7] C. Fabiani, A.L. Pisello, E. Bou-Zeid, J. Yang, F. Cotana, Adaptive measures for mitigating urban heat islands: the potential of thermochromic materials to control roofing energy balance, Appl. Energy 247 (2019) 155–170, https://doi.org/10.1016/j.apenergy.2019.04.020.
[8] U. Berardi, M. Garai, T. Morselli, Preparation and assessment of the potential energy savings of thermochromic and cool coatings considering inter-building

effects, Sol. Energy 209 (2020) 493–504, https://doi.org/10.1016/j.solener.2020.09.015.
[9] Y. Zhang, Y. Zhang, J. Yang, X. Zhang, Energy saving performance of thermochromic coatings with different colors for buildings, Energy Build. 215 (2020) 1–11, https://doi.org/10.1016/j.enbuild.2020.109920.
[10] E.C. Sánchez, D.M. Vilà, Thermochromic materials as passive roof technology: their impact on building energy performance, Energies 15 (6) (2022) 2161, https://doi.org/10.3390/en15062161.
[11] G. Song, K. Zhang, F. Xiao, Z. Zhang, S. Jiao, Y. Gong, Building energy efficiency enhancement through thermochromic powder-based temperature-adaptive radiative cooling roofs, Buildings 14 (6) (2024) 1745, https://doi.org/10.3390/buildings14061745.
[12] N. Guo, S. Liu, C. Chen, S. Song, H. Mo, M. Yan, M. Chen, Outdoor adaptive temperature control based on a thermochromic hydrogel by regulating solar heating, Sol. Energy 270 (2024), https://doi.org/10.1016/j.solener.2024.112405.
[13] C.C. de Azevedo, D.N. Amorim, M. Santamouris, Use of passive cooling techniques and super cool materials to minimize cooling energy and improve thermal comfort in Brazilian schools, Energy Build. 312 (2024), https://doi.org/10.1016/j.enbuild.2024.114125.
[14] A. Kitsopoulou, E. Bellos, C. Sammoutos, P. Lykas, M.G. Vrachopoulos, C. Tzivanidis, A detailed investigation of thermochromic dye-based roof coatings for Greek climatic conditions, J. Build. Eng. 84 (2024) 108570, https://doi.org/10.1016/j.jobe.2024.108570.
[15] E. Badino, G. Autretto, S. Fantucci, V. Serra, M. Zinzi, Development of testing procedures for assessing the thermal and optical performance of thermochromic coatings for buildings, Sol. Energy 263 (2023) 111950, https://doi.org/10.1016/j.solener.2023.111950.
[16] J. Hu, X.B. Yu, Adaptive thermochromic roof system: assessment of performance under different climates, Energy Build. 192 (2019) 1–14, https://doi.org/10.1016/j.enbuild.2019.02.040.
[17] J. Hu, X.B. Yu, Design and characterization of energy efficient roofing system with innovative TiO2 enhanced thermochromic films, Constr. Build. Mater. 223 (2019) 1053–1062, https://doi.org/10.1016/j.conbuildmat.2019.06.003.
[18] Y. Zhang, H. Liu, J. Niu, X. Wang, D. Wu, Development of reversible and durable thermochromic phase-change microcapsules for real-time indication of thermal energy storage and management, Appl. Energy 264 (2020) 114729, https://doi.org/10.1016/j.apenergy.2020.114729.
[19] M. Hussain, A.M. Sikandar, S. Nasir, W. Ahmed, Effect of SiO2 coated leuco-dye based thermochromic pigment on the properties of Portland cement pastes, J. Build. Eng. 35 (2021), https://doi.org/10.1016/j.jobe.2020.102019.
[20] H. Cheng, F. Wang, H. Liu, J. Ou, W. Li, R. Xue, Fabrication and properties of thermochromic superhydrophobic coatings, Adv. Eng. Mater. 24 (2022) 2100647, https://doi.org/10.1002/adem.202100647.
[21] Y. Li, Z. Jiang, F. He, X. Chen, P. Li, G. Wang, X. He, W. Zhu, Reversible thermochromic microcapsules with SiO2 shell for indicating temperature and thermoregulation, J. Energy Storage 72 (D) (2023), https://doi.org/10.1016/j.est.2023.108674.
[22] S. Bhupathi, S. Wang, Y. Ke, Y. Long, Recent progress in vanadium dioxide: the multi-stimuli responsive material and its applications, Mater. Sci. Eng. R Rep. 155 (2023) 100747, https://doi.org/10.1016/j.mser.2023.100747.
[23] M. Casini, Chapter 7 - advanced construction materials, in: M. Casini (Ed.), Construction 4.0, Woodhead Publishing, 2022, pp. 337–404, https://doi.org/10.1016/B978-0-12-821797-9.00005-2.
[24] M. Aburas, V. Soebarto, T. Williamson, R. Liang, H. Ebendorff-Heidepriem, Y. Wu, Thermochromic smart window technologies for building application: a review, Appl. Energy 255 (2019) 113522, https://doi.org/10.1016/j.apenergy.2019.113522.
[25] L. Giovannini, F. Favoino, V.R.M. Pellegrino, V. Lo Verso, M. Serra, M. Zinzi, Thermochromic glazing performance: from component experimental characterisation to whole building performance evaluation, Appl. Energy 251 (2019) 113335, https://doi.org/10.1016/j.apenergy.2019.113335.
[26] M. Aburas, H. Ebendorff-Heidepriem, M. Lei, J. Li, T. Zhao, Y. Williamson, V. Wu, V. Soebarto, Smart windows – transmittance tuned thermochromic coatings for dynamic control of building performance, Energy Build. 235 (2021) 110717, https://doi.org/10.1016/j.enbuild.2021.110717.
[27] K. Khaled, U. Berardi, Z. Liao, Energy modelling and saving potential of polymeric solar-responsive thermochromic window films, Sol. Energy 244 (2022) 84–103, https://doi.org/10.1016/j.solener.2022.08.008.
[28] M. Fahland, J. Szelwicka, W. Langgemach, Energy-saving potential of thermochromic coatings in transparent building envelope components, J. Facade Des. Eng. 11 (2) (2023) 197–210, https://doi.org/10.47982/jfde.2023.2.A5.
[29] K. Khaled, U. Berardi, Z. Liao, Energy-saving potential of thermochromic glazing in a cold climate, in: L.L. Wang, et al. (Eds.), Proceedings of the 5th International Conference on Building Energy and Environment. COBEE 2022, Environmental Science and Engineering, 2023, pp. 91–100, https://doi.org/10.1007/978-981-19-9822-5_9. Springer.
[30] S. Wu, H. Sun, M. Duan, H. Mao, Y. Wu, H. Zhao, B. Lin, Applications of thermochromic and electrochromic smart windows: materials to buildings, Cell Reports Phys. Sci. 4 (5) (2023) 101370, https://doi.org/10.1016/j.xcrp.2023.101370.
[31] C. Jiang, L. He, Q. Xuan, et al., Phase-change VO2-based thermochromic smart windows, Light Sci. Appl. 13 (2024) 255, https://doi.org/10.1038/s41377-024-01560-9.
[32] A.C. Hidalgo-Araujo, R. Salomão, K.A. Dornelles, Application of thermochromic and self-cleaning materials in buildings: a bibliometric analysis, in: U. Berardi (Ed.), Multiphysics and Multiscale Building Physics. IABP 2024. Lecture Notes in Civil Engineering, vol. 552, Springer, 2025, pp. 651–663, https://doi.org/10.1007/978-981-97-8305-2_56.
[33] A.C. Hidalgo-Araujo, R. Salomão, U. Berardi, K.A. Dornelles, Thermochromic materials for building applications: overview through a bibliometric analysis, Sol. Energy 293 (2025) 113491, https://doi.org/10.1016/j.solener.2025.113491.
[34] P. Sirvent, G. Perez, A. Guerrero, VO2 sprayed cementitious materials for thermochromic building envelopes, Sol. Energy 243 (2022) 13–21, https://doi.org/10.1016/j.solener.2022.07.040.
[35] G. Perez, I. Galan, J.L.G. Calvo, K. Lontschar, A. Guerrero, Chemical and physical effects of the addition of thermochromic VO2 particles to cement, Mater. Chem. Phys. 322 (2024) 129587, https://doi.org/10.1016/j.matchemphys.2024.129587.
[36] I. Top, R. Binions, M.E.A. Warwick, C.W. Dunnill, M. Holdynski, I. Abrahams, VO2/TiO2 bilayer films for energy efficient windows with multifunctional properties, J. Mater. Chem. C 6 (16) (2018) 4485–4493, https://doi.org/10.1039/C8TC00835C.
[37] J. Pi, C.-B. Li, R.-Y. Sun, L.-Y. Li, F. Wang, F. Song, J.-M. Wu, X.-L. Wang, Y.-Z. Wang, Superhydrophobic and thermochromic VO2-based composite coatings for energy-saving smart windows, Compos. Commun. 32 (2022) 101167, https://doi.org/10.1016/j.coco.2022.101167.
[38] Y. Liu, R. Sun, B. Jin, T. Li, L. Yao, L. Feng, J. He, Superhydrophobic VO2 nanoparticle/PDMS composite films as thermochromic, anti-icing, and self-cleaning coatings, ACS Appl. Nano Mater. 5 (4) (2022) 5599–5608, https://doi.org/10.1021/acsanm.2c00562.
[39] K. Khaled, U. Berardi, M. Schlaf, D. Soldatov, One-step hydrothermal synthesis of vanadium dioxide structures for thermochromic glass applications, Multiphy. Multiscale Build. Phys. IABP 552 (2025) 749–762, https://doi.org/10.1007/978-981-97-8305-2_49. Springer.
[40] S. Soudian, U. Berardi, N.O. Laschuk, Effects of long-term UV exposure on the performance of cement plasters integrated with thermochromic paint and PCMs for building facade applications, in: C. Serrat, J.R. Casas, V. Gibert (Eds.), Proceedings of the XV International Conference on Durability of Building Materials and Components (DBMC 2020), 2020, pp. 1–10, https://doi.org/10.23967/dbmc.2020.163. Barcelona, Spain.
[41] Y. Xi, S. Xu, J. Zhang, Reversible thermochromic composites for intelligent adjustment of solar reflectance, Mater. Chem. Phys. 276 (2022) 125372, https://doi.org/10.1016/j.matchemphys.2021.125372.
[42] S. Wang, H. Xu, X. Zhang, S. Yang, X. Jiang, 2D ordered porous VO_2-based composite film with enhanced thermochromism performance and high stability for smart windows, Ceram. Int. 50 (19, Part A) (2024) 35265–35272, https://doi.org/10.1016/j.ceramint.2024.06.336.
[43] H. Xu, S. Wang, X. Zhang, S. Yang, R. Hu, T. Liu, X. Jiang, X. Yu, Coordination compound guided a novel composite film with $Zn_2V_2O_7$ nanoflake and VO_2@$Zn_2V_2O_7$ nanoparticle for enhanced thermochromism smart window, Small 20 (23) (2024) 2312004, https://doi.org/10.1002/smll.202312004.
[44] S. Liu, Y. Li, Y. Wang, Y. Du, K.M. Yu, H.-L. Yip, A.K.Y. Jen, B. Huang, C.Y. Tso, Mask-inspired moisture-transmitting and durable thermochromic perovskite smart windows, Nat. Commun. 15 (1) (2024) 876, https://doi.org/10.1038/s41467-024-45047-y.
[45] X. Sun, Y. Wu, S. Tang, Self-adaptive smart thermochromic film with quick response for all-year radiative cooling and solar heating, ACS Appl. Mater. Interfaces 16 (49) (2024) 68407–68415, https://doi.org/10.1021/acsami.4c16273.
[46] S.R. Dantas, F. Vittorino, Comparison of reflectance to solar radiation between mortars treated with TiO2 and painted mortars after three years of exposure, J. Build. Eng. 46 (2022), https://doi.org/10.1016/j.jobe.2021.103829.
[47] K. Wang, M. Janczarek, Z. Wei, T. Raja-Mogan, M. Endo-Kimura, T.M. Khedr, B. Ohtani, E. Kowalska, Morphology- and crystalline composition-governed activity of titania-based photocatalysts: overview and perspective, Catalysts 9 (2019) 1054.
[48] X. Guo, L. Rao, P. Wang, C. Wang, T. Ao, W. Jiang, Y. Wang, Photocatalytic properties of P25-doped TiO2 composite film synthesized via sol-gel method on cement substrate, J. Environ. Sci. 66 (2018) 71–80, https://doi.org/10.1016/j.jes.2017.05.029.
[49] J. Papac, S. Garcia Ballesteros, S. Tonkovic, M. Kovacic, A. Tomic, M. Cvetnić, H. Kusic, I. Senta, S. Terzić, M. Ahel, Z. Wang, A. Loncaric Bozic, Degradation of pharmaceutical memantine by photo-based advanced oxidation processes: kinetics, pathways and environmental aspects, J. Environ. Chem. Eng. 11 (2) (2023) 109334, https://doi.org/10.1016/j.jece.2023.109334.
[50] P. García-Negueroles, S. García-Ballesteros, L. Santos-Juanes, C. Sabater, M. A. Castillo, M.F. López-Pérez, R. Vicente, A.M. Amat, A. Arques, Humic like substances extracted from oil mill wastes in photo-Fenton processes: characterization, performance and toxicity assessment, J. Environ. Chem. Eng. 9 (6) (2021) 106862, https://doi.org/10.1016/j.jece.2021.106862.
[51] S. Domenici, R. Speranza, F. Bella, A. Lamberti, T. Gatti, A sustainable hydrogel-based dye-sensitized solar cell coupled to an integrated supercapacitor for direct indoor light-energy storage, Sol. RRL 9 (2025) 2570061, https://doi.org/10.1002/solr.202570061.
[52] M. Bonomo, A.Y. Segura Zarate, L. Fagiolari, A. Damin, S. Galliano, C. Gerbaldi, F. Bella, C. Barolo, Unreported resistance in charge transport limits the photoconversion efficiency of aqueous dye-sensitised solar cells: an electrochemical impedance spectroscopy study, Mater. Today Sustain. 21 (2023) 100271, https://doi.org/10.1016/j.mtsust.2022.100271.
[53] G. Gianola, R. Speranza, F. Bella, A. Lamberti, Homo-tandem-bifacial dye-sensitized solar cell: a new paradigm to boost photoconversion efficiency above limit, Sol. Energy 265 (2023) 112116, https://doi.org/10.1016/j.solener.2023.112116.

[54] C.J. Brinker, G.W. Scherer, Particulate sols and gels, in: C.J. Brinker, G.W. Scherer (Eds.), Sol-gel Science, Academic Press, 1990, pp. 234–301, https://doi.org/10.1016/B978-0-08-057103-4.50009-X.
[55] C.J. Brinker, G.W. Scherer, Film formation, in: C.J. Brinker, G.W. Scherer (Eds.), Sol-gel Science, Academic Press, 1990, pp. 786–837, https://doi.org/10.1016/B978-0-08-057103-4.50018-0.
[56] Y. Wei, Q. Wu, H. Meng, Y. Zhang, C. Cao, Recent advances in photocatalytic self-cleaning performances of TiO_2-based building materials, RSC Adv. 13 (30) (2023) 20584–20597, https://doi.org/10.1039/D2RA07839B.
[57] ASTM, ASTM E1876-22 - Standard Test Method for Dynamic Young's Modulus, Shear Modulus, and Poisson's Ratio by Impulse Excitation of Vibration, American Society for Testing and Materials, 2022.
[58] ASTM, ASTM E903–20 - Standard Test Method for Solar Absorptance, Reflectance and Transmittance of Materials Using Integrating Spheres, American Society for Testing and Materials, 2020.
[59] ASTM, ASTM G173–23 - Standard Tables for Reference Solar Spectral Irradiances: Direct Normal and Hemispherical on 37° Tilted Surface, American Society for Testing and Materials, 2023.
[60] ASTM, ASTM E1933: Standard Practice for Measuring and Compensating for Emittance Using Infrared Imaging Radiometers, American Society for Testing and Materials, 2018.
[61] ASTM, ASTM D7334-08: Standard Practice for Surface Wettability of Coatings, Substrates, and Pigments by Advancing Contact Angle Measurement, American Society for Testing and Materials, 2008.
[62] R. Levinson, P. Berdahl, H. Akbari, Solar spectral optical properties of pigments—Part II: survey of common colorants, Sol. Energy Mater. Sol. Cell. 89 (4) (2005) 351–389, https://doi.org/10.1016/j.solmat.2004.11.013.
[63] ISO, ISO 80004-1:2023(en) – Nanotechnologies – Vocabulary – Part 1: Core vocabulary, International Organization for Standardization, 2023.
[64] R.K. Iler, The Chemistry of Silica: Solubility, Polymerization, Colloid and Surface Properties, and Biochemistry of Silica, Wiley, 1979.
[65] W. Xu, K. Li, Y. Li, Y. Sun, Y. Bao, D. Wan, X. Tan, D. Hao, Surface strengthening of building tiles by ion exchange with adding molten salt of KOH, Int. J. Appl. Ceram. Technol. 19 (3) (2022) 1490–1497, https://doi.org/10.1111/ijac.14003.
[66] ASTM, ASTM D7897-18 (Reapproved 2023) - Standard Practice for Laboratory Soiling and Weathering of Roofing Materials to Simulate Effects of Natural Exposure on Solar Reflectance and Thermal Emittance, American Society for Testing and Materials, 2023.
[67] A.C.H. Araujo, Solar Absorptance and the Natural Aging of Roof Tiles Exposed to Weather, Institute of Architecture and Urbanism, University of São Paulo, 2022, https://doi.org/10.11606/D.102.2022.tde-06062022-143613. São Carlos.